Bharti Kumari[a], Daniel John[a], Paul Hoffmann, Anne Spende, Maria Eugenia Toimil-Molares, Christina Trautmann, Christian Hess, Philip Ruff, Marcus Schulze, Robert Stark, Gerd Buntkowsky*, Annette Andrieu-Brunsen and Torsten Gutmann*

Surface Enhanced DNP Assisted Solid-State NMR of Functionalized SiO_2 Coated Polycarbonate Membranes

https://doi.org/10.1515/zpch-2017-1032
Received September 8, 2017; accepted February 14, 2018

Abstract: Surface enhanced solid-state NMR by dynamic nuclear polarization (DNP SENS) enables the characterization of the inner-pore surface functionalization of porous etched ion-track membranes exhibiting low specific surface areas compared to typical SBA- or MCM-type mesoporous silica materials. The membranes were conformally coated with a 5 nm thin SiO_2 layer by atomic layer deposition. This layer was subsequently modified by aminopropyl silane linkers that allow further functionalization via the terminal amine group. The results evidence that in principle DNP SENS is a capable tool to analyze more complex porous systems, e.g. bioinspired functional etched ion-track membranes down to the molecular level. These results are relevant also for single nanopore systems,

[a]**Bharti Kumari and Daniel John:** These authors contributed equally to this work.
***Corresponding authors: Gerd Buntkowsky and Torsten Gutmann,** Eduard-Zintl Institute for Inorganic and Physical Chemistry, Technische Universität Darmstadt, Alarich-Weiss-Str. 8, D-64287 Darmstadt, Germany, e-mail: gerd.buntkowsky@chemie.tu-darmstadt.de (G. Buntkowsky); gutmann@chemie.tu-darmstadt.de (T. Gutmann)
Bharti Kumari, Christian Hess and Philip Ruff: Eduard-Zintl Institute for Inorganic and Physical Chemistry, Technische Universität Darmstadt, Alarich-Weiss-Str. 8, D-64287 Darmstadt, Germany
Daniel John and Annette Andrieu-Brunsen: Ernst-Berl Institute for Chemical Engineering and Macromolecular Science, Technische Universität Darmstadt, Alarich-Weiss-Str. 4, D-64287 Darmstadt, Germany
Paul Hoffmann, Anne Spende and Christina Trautmann: GSI Helmholtzzentrum für Schwerionenforschung GmbH, Planckstr. 1, D-64291 Darmstadt, Germany; and Materialwissenschaft, Technische Universität Darmstadt, Alarich-Weiss-Str. 2, D-64287 Darmstadt, Germany
Maria Eugenia Toimil-Molares: Materialwissenschaft, Technische Universität Darmstadt, Alarich-Weiss-Str. 2, D-64287 Darmstadt, Germany
Marcus Schulze and Robert Stark: Physics of Surfaces, Institute of Materials Science and Center of Smart Interfaces, Technische Universität Darmstadt, Alarich-Weiss-Str. 16, D-64287 Darmstadt, Germany

for which a direct analysis of the channel surface functionalization is not feasible by classical characterization methods. The applicability of DNP SENS to complex porous systems requires the optimization of the sample preparation and measurement parameters.

Keywords: dynamic nuclear polarization; etched ion-track membranes; silica coating; solid-state NMR; surface analysis.

1 Introduction

Etched ion-track membranes based on polycarbonate (PC) or polyethylene terephthalate (PET), are powerful systems for the investigation of new technologies in various fields such as nanofluidics and sensing nanodevices. Multipore etched membranes exhibit pore surfaces with different functionalities and have recently been applied for ion current gating and ion adsorption [1, 2] as well as for nanowire synthesis [3, 4]. In addition, single channel polymer membranes [5, 6] have been functionalized by various surface modification approaches, and successfully applied to detect among others, e.g. DNA, γ-D-glutamic acid, streptavidin, immunoglobulin G, ricin, or hydrogen peroxide [7–9].

Etching of ion-tracks leads to porous membranes with narrow pore size distribution [10]. Subsequently, such membranes can be conformally coated by atomic layer deposition (ALD). In this case, the resulting channels may exhibit various compositions (e.g. SiO_2, Al_2O_3, TiO_2), and tuneable diameter and aspect ratio [11]. It has recently been shown that both thickness of the silica layer as well as the hydrophilicity of the membrane are adjustable by the number of ALD cycles [12]. In addition, the thin silica wall bears free silanol groups that allow a further binding of organic functional groups or molecules by a post-grafting approach.

In general, a current challenge in the field is to develop methods that allow us to directly prove the post-functionalization of the pore surfaces, in particular in case of covalent grafting. Vibrational spectroscopy techniques enable the detection of changes of the molecular structure occurring by functionalization, however the spectra interpretation may be challenging in case of overlapping vibration bands. Solid-state NMR is an alternative method to partially overcome this issue since it enables the separate detection of different nuclei (i.e. ^{13}C, ^{29}Si and ^{15}N), each containing an individual chemical shift range allowing the detailed analysis of the chemical environment in their vicinity. However, conventional solid-state NMR suffers from its low intrinsic sensitivity which in the past limited its application to systems with high specific surface areas (>30 m^2/g) such as functionalized SBA and MCM type mesoporous silica materials containing relatively large grafting densities of functional groups (see Refs. [13–18] and

references therein). Recently, in the pioneering works by Emsley and Griffin a novel approach of solid-state NMR combined with dynamic nuclear polarization (DNP) was demonstrated to drastically enhance the signals of surface functional groups on silica materials [19, 20]. This technique seems to be robust for the characterization of more challenging systems as it has been later presented for a number of inorganic/organic functional silica hybrid materials [21–41]. Furthermore, as it has been very recently shown for polymer samples as well as for functionalized paper substrates, it enables the selective signal enhancement of functional groups/domains [42, 43]. Such an approach facilitates differentiating the signals of functional groups from those of the carrier material.

The aim of the present work is to apply the DNP SENS technique that is surface sensitive to identify the pore wall modification of SiO_2 coated etched ion-track nanochannels. Here, both 3-aminopropyldimethylmethoxy silane (APDMS) and 3-aminopropyltriethoxy silane (APTES) are used to modify the silica coated membranes with amino end functionalized silanes under dry conditions [44]. The ^{29}Si solid-state spectra of the resulting systems are expected to be highly sensitive to changes upon functionalization of the SiO_2 layered etched ion-track membranes.

2 Experimental details

2.1 Preparation of etched ion-track polycarbonate membranes

Etched ion-track membranes were fabricated by swift heavy ion irradiation and chemical etching. Polycarbonate foils based on bisphenol A (30 μm, Makrofol N, Bayer AG) were irradiated with Au ions having energies of ~2 GeV at the UNILAC accelerator of the Helmholtz Center for Heavy Ion Research. The irradiation was done under 45° incidence angle in four sequential steps. After each step, the foil was turned by 90° around the foil normal to irradiate the sample from four different directions. During irradiation, each ion generates a highly localized cylindrical damage zone in the foil called ion-track. Subsequently, the ion-tracks are selectively dissolved and enlarged to form nanochannels. Thus, the density of channels is defined by the total ion fluence during irradiation, i.e. the sum of the fluences for each direction. In this work, the foils were irradiated with $\sim 2 \cdot 10^9$ ions/cm^2 from each direction, the resulting channel density being namely $\sim 8 \cdot 10^9$ cm^{-2}. Chemical etching was performed by immersing the foils in a 6 mol/L NaOH solution at 50 °C for ~288 s, resulting in templates with interconnected cylindrical channels with diameter ~95 nm [45, 46]. Prior to the etching, the irradiated foils were exposed to UV light for 1 h on each side.

2.2 Atomic layer deposition (ALD): SiO_2 coating

Conformal SiO_2 films were deposited using a self-made stainless steel ALD reactor operating at a pressure of 1.3 Torr. For SiO_2 depositions the reactor walls were heated to 60 °C (substrate temperature ~55 °C). $SiCl_4$ (Sigma-Aldrich, 99.9%) and water were employed as precursors and inserted into the 3 L volume reaction chamber by evaporation. The application of the precursors was controlled by setting the valve opening time to 0.1 s for each precursor. Precursor exposures were set to 1 min during each half cycle of the cyclic ABAB type like process. The reaction was then terminated by 1 min purging with N_2 (99.999%, 200 mL/min). Pyridine was used as a catalyst and fed into the reactor prior to precursor exposure.

For the deposition of 5 nm SiO_2 on etched ion-track polycarbonate (PC) membranes 28 ALD cycles were applied. The growth rate of the SiO_2 film regarding the reaction of $SiCl_4$ and H_2O was determined by small angle X-ray scattering (SAXS) as 1.8 Å/cycle according to Ref. [12].

2.3 Functionalization with 3-aminopropyldimethyl methoxysilane (APDMS)

The SiO_2-coated polycarbonate membrane was placed into a 0.1 weight-% ethanolic (absolute EtOH) solution of 3-aminopropyldimethyl-methoxysilane located in a flame-dried nitrogen flushed Schlenk flask and kept at 60 °C for 1 h. Unreacted 3-aminopropyldimethyl methoxysilane was removed by extraction in ethanol for 15 min.

2.4 Functionalization with 3-aminopropyl triethoxysilane (APTES)

3-Aminopropyl triethoxysilane (3.3 µL; 14 nmol) was dissolved in absolute ethanol (40 mL) in a flame dried, nitrogen flushed Schlenk flask. The mixture was heated to 70 °C under mild stirring before adding the SiO_2-coated polycarbonate membrane. The reaction was allowed to proceed for 2 h followed by a thermal treatment of the foil at 70 °C for 1 h. The foil was extracted in ethanol for 15 min, dried at ambient conditions and stored in a brown glass bottle.

2.5 Atomic force microscopy (AFM)

A Dimension Icon (Bruker, Billerica, MA, USA) was used for the atomic force microscope measurements. For imaging the Peak Force Tapping mode was

applied using Scan Asyst Fluid+ cantilever (Bruker, Billerica, MA, USA) with a nominal force constant of 0.7 N/m and a nominal resonant frequency of 150 kHz in air. For every sample, images with a size of 5×5 μm^2 and 500×500 nm^2 (512×512 data points) were taken with a scan frequency of 0.5 Hz. The frequency of the extend-retract cycles was 1 kHz, the maximum force was limited to 2 nN. Calibration was done with the inbuilt calibration procedure based on five deflection vs. distance curves taken on a sapphire surface. The engage set point was set smaller than the Peak Force. All AFM images were processed with a second order XY plane fit.

The estimation of the pore size was carried out with the inbuilt particle analysis tool. In each 5×5 μm^2 image 90 cavities, that were considered to be created by a single ion impact, were analyzed and their diameter and area were assessed.

2.6 Sample preparation for DNP SENS measurements

For all samples, the polymer foil was cut into small pieces. 15–20 mg were wetted with 15–20 µL of a radical solution containing 15 mM AMUPol in glycerol-d_8/D_2O/H_2O (60/30/10 w/w/w), and filled in a 3.2 mm sapphire rotor.

2.7 DNP SENS experiments

DNP SENS experiments were carried out on a Bruker Ascend 400 DNP AVANCE III spectrometer equipped with a low temperature MAS triple resonance ^1H/X/Y probe, and a 9.7 T Bruker gyrotron system corresponding to a microwave frequency of 263 GHz. The low-temperature measurements were operated at a frequency of 400.02 MHz for ^1H, 100.59 MHz for ^{13}C and 79.47 MHz for ^{29}Si at a temperature of nominally 110 K. At this temperature 3.2 mm rotors equipped with ZrO_2 caps were used. The ^{29}Si CP MAS and ^{13}C CP MAS experiments were performed at 8 kHz spinning employing contact times of 3 ms and 2 ms, respectively, with a repetition delay of 1.3 times T_1 of the protons for each sample. The decoupling schemes tppm15 [47] and SPINAL64 [48] were utilized for ^{13}C CP and ^{29}Si CP MAS experiments, respectively, during data acquisition. Some of these experiments were repeated at 9 and 10 kHz spinning to distinguish spinning sidebands from isotropic signals. Spectra were referenced employing trimethylsilyl propanoic acid (TSP) (measured at nominally 110 K) as external standard where ^1H was set to 0 ppm and ^{29}Si was set to 0 ppm. Similarly, ^{13}C-^{15}N glycine in 20 mM TOTAPOL in glycerol-d_8/H_2O/D_2O (60/30/10 w/w/w) was used for referencing ^{13}C spectra where the ^{13}C signal of the CO group was set to –176.5 ppm.

The enhancement factors were calculated according to Ref. [42] by comparing the intensity of the signals in the MW on and the MW off spectra measured and processed with the same parameters. The error bars were determined from the height of the noise level of the spectra.

2.8 Scanning electron microscopy (SEM)

The scanning electron micrographs were obtained using a Philips XL30 FEG high resolution scanning electron microscope. Prior to characterization, the samples were prepared by sputtering a thin Au layer for 20 s to prevent unwanted charging effects. An acceleration voltage of 10 kV and a working distance of 6.3 mm were used.

3 Results and discussion

3.1 Atomic force microscopy (AFM)

Stability and morphology of the etched ion-track membrane surface were monitored after each modification step (Scheme 1) by atomic force microscopy (AFM). Figure 1a displays the untreated polycarbonate etched ion-track membrane, while Figure 1b,c show the same membrane after SiO_2 coating and after subsequent functionalization with APTES linker, respectively. These images demonstrate that membrane and pore openings stay intact during these modification steps. The analysis of the pore diameters based on the AFM images (ESI Table S1) reveals an expected decrease of the average pore size after SiO_2 layering and functionalization. These AFM images underline the successful modification of the membranes in a qualitative manner. However, a quantitative evaluation of pore diameter and silica layer thickness is challenging due to the well-known influence of the AFM tip size. In any case, assuming that the AFM tip can be approximated as a sphere with a diameter of approximately 20 nm, a pore diameter of ~85–95 nm would be visualized as ~70 nm, in agreement with the diameters derived from the images (ESI Table S1) that are in the range of 68–72 nm.

3.2 ^{29}Si CP MAS DNP SENS

Prior to any chemical functionalization of the SiO_2 coated PC membrane, the suitability of the DNP SENS technique to enhance signals of the thin SiO_2 membrane

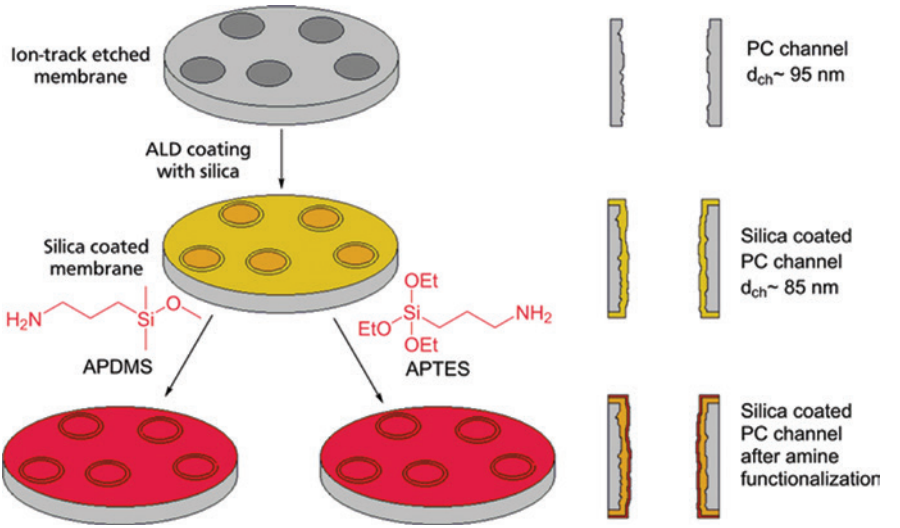

Scheme 1: Illustration of the steps implemented to prepare amine functionalized silica coated porous membranes.

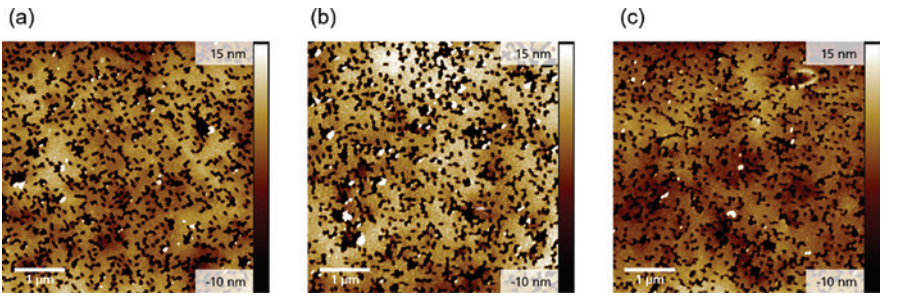

Fig. 1: AFM images in peak force tapping mode of (a) a polycarbonate etched ion-track membrane, (b) a SiO_2 coated membrane and (c) an APTES functionalized SiO_2 coated membrane.

coating layer was tested by comparing the ^{29}Si CP MAS spectra measured with and without microwave (MW on and MW off). This reveals an enhancement factor of 7.0 ± 3.3 (see Figure S1a,b). The MW on spectrum (ESI Figure S1b) exhibits clearly distinguishable signals in the range between –90 ppm and –115 ppm, which are typical for Q_n groups ($Q_2 = -99$ ppm, $Q_3 = -104$ ppm, $Q_4 = -112$ ppm). Their presence indicates the formation of a silica layer containing structural features comparable to mesoporous SiO_2 [49].

To investigate the pore wall modification of the SiO_2 coating layer on the polycarbonate membranes, the SiO_2 coated membranes were subjected to

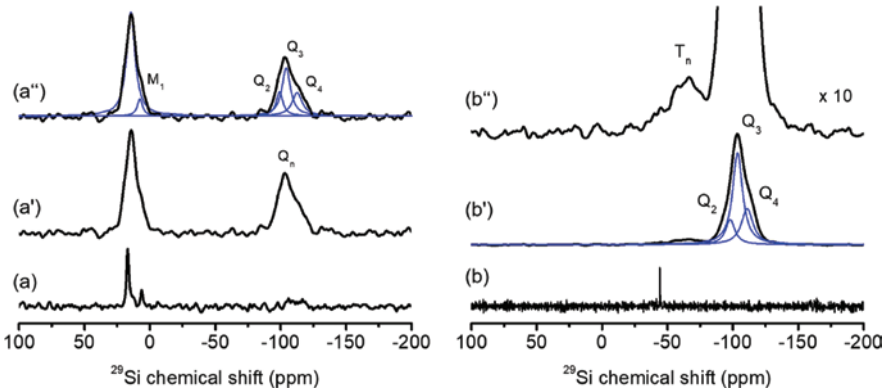

Fig. 2: Static ^{29}Si spectra of the free linkers: APDMS (a) and APTES (b). ^{29}Si CP-MAS spectra of the functionalized polycarbonate membranes measured at 8 kHz spinning, nominally 110 K, and with MW on: functionalization with APDMS (a′) and functionalization with APTES (b′). Spectrum (a″) shows the deconvolution of (a′) and spectrum (b″) zooms into spectrum (b′) by a factor of 10 to illustrate the occurrence of T_n groups. Note: Deconvolutions were done employing Lorentzian–Gaussian lines. Both samples were impregnated with 15 mM AMUPol in glycerol-d_8/D_2O/H_2O.

linker molecules, and the corresponding ^{29}Si CP MAS DNP SENS spectra were recorded. As starting point, the functionalization with APDMS was investigated since this linker molecule can form only one bond to the surface of the SiO_2 coated membrane. The ^{29}Si CP MAS spectra of the APDMS functionalized membrane in Figure 2a′ and a″ reveal, as expected, Q_n groups between –90 ppm and –115 ppm corresponding to the presence of the silica layer. More importantly, an additional signal is observed between +5 and +20 ppm, which contains at least two single lines centered at +15 and +7 ppm (Figure 2a″). Compared with the signals obtained for the free APDMS linker (+17 and +6 ppm) (Figure 2a) no significant differences of the chemical shifts are obtained after reaction of the linker with the SiO_2 layered membrane, while a significant broadening of the signals occurrs. This indicates that APDMS linker molecules are interacting with the SiO_2 coated etched ion-track membrane. The obtained signals most probably refer to covalently bound APDMS linker whose signal is expected at +13 ppm. (M_1 group according to Ref. [50], ESI Figure S2). However, adsorbed or encapsulated APDMS linker molecules cannot be fully excluded which would also lead to signals in the range between +7 ppm and +15 ppm. As the chemical shift differences between free, covalently bound, adsorbed or encapsulated APDMS are small, a second set of experiments using APTES instead of APDMS functionalization has been investigated. In the spectrum of the APTES functionalized SiO_2

layered membrane (Figure 2b″), a signal between –50 ppm and –75 ppm (typical range of T_n groups according to Ref. [49], ESI Figure S2) is observed. This signal is shifted to lower ppm values compared to the free linker (ca. –47 ppm, Figure 2b) and thus clearly demonstrates the successful covalent binding of the APTES linker on the silica surface.

3.3 ^{13}C CP MAS DNP SENS

^{13}C CP MAS spectra were recorded to shed more light on the organic components of the functionalized SiO_2 layered membrane. Comparison between the MW on and MW off ^{13}C CP MAS spectra (Figure 3a,b) reveals significantly different signal enhancements for various functional groups present in the sample. For the ^{13}C signal of glycerol-d_8 of the solvent matrix at 65 ppm a drastic signal enhancement of about 100 is obtained, while only a low enhancement of 1.8 ± 0.1 is observed for the signals at 120–135 ppm assigned to the aromatic moieties of the polycarbonate foil. This strong difference in the signal enhancements most probably originates

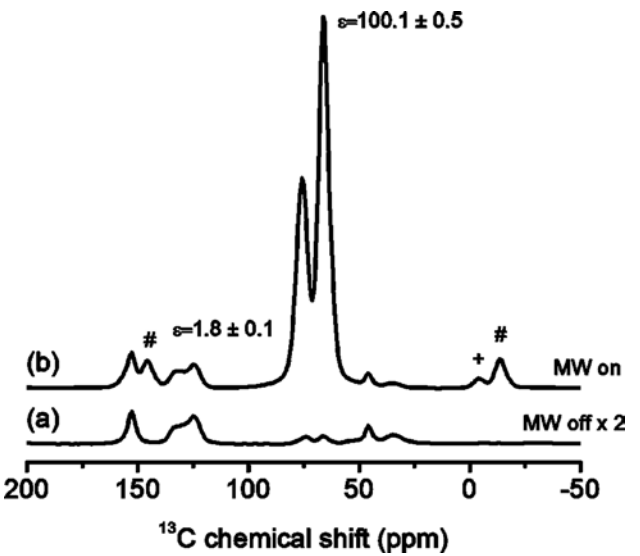

Fig. 3: ^{13}C CP MAS spectra of the SiO_2 ALD coated polycarbonate membrane, measured at 8 kHz spinning, nominally 110 K, for (a) MW on and (b) MW off, revealing signal enhancements. Note: Signals marked with + or # are spinning sidebands of the glycerol. Signals obtained between 25 and 50 ppm refer to aliphatic groups of the diphenyl-dimethyl-methane units, and the signal at 152 refers to the carbamate groups occurring in the polycarbonate foil.

from the compatibility of the solvent matrix employed for the DNP sample preparation and the polycarbonate foil. This is consistent with the fact that ALD provides a conformal layer inside the nanochannels of etched ion-track membranes, as demonstrated previously [11, 12]. This SiO_2 layer is expected to restrict the ^1H-^1H spin diffusion and thus causes only an insignificant signal enhancement of the functional groups of the polycarbonate. On the other hand, the strong signal enhancement of the hydrophilic glycerol-d_8 solvent matrix induces a significant enhancement of hydrophilic functional groups on the surface of the SiO_2 coated membranes which may explain the above-mentioned signal enhancement (7.0 ± 3.3) of the Q-groups of the silica layer in the ^{29}Si CP MAS spectra. Surprisingly, this signal enhancement in the ^{29}Si CP MAS is lower than the enhancement obtained for the glycerol-d_8 of the solvent matrix as well as the signal enhancement (ca. 50) typically obtained for ^{29}Si of porous silica materials [26, 33]. One possible explanation for this phenomenon is related to the ALD coating process which may induce defect Si sites containing OH in the bulk of the 5 nm SiO_2 layer. Such sites are not hyperpolarized but produce a thermal signal that is visible also in the MW off spectrum. This hypothesis is underlined by the MW off spectrum represented in ESI Figure S1a that clearly shows signals of Q_2 and Q_3 groups that are most probably related to Si sites containing OH in the bulk since the amount of surface Si–OH sites is assumed to be below the detection limit in case of our small surface area membrane system. As a consequence, the calculated enhancement factor obtained as ratio of the intensities of the MW on and MW off spectrum is lowered compared to porous silica materials.

Comparing the ^{13}C CP MAS DNP SENS spectra of the silica coated membrane before and after functionalization with APTES (ESI Figure S3b,c) or APDMS (ESI Figure S3e,f) it is initially surprising that for the APTES linker system no additional signals (expected between 0 and 50 ppm, ESI Figure S3a) are obtained after surface functionalization. The disappearance of the signals of the ethoxy groups at ca. 18 and 58 ppm in the ^{13}C CP MAS DNP SENS spectrum (ESI Figure S3c) suggest their hydrolysis, which enables the linker molecules to bind on the surface of the SiO_2 coated membrane. This is underlined by the deeper analysis of the ^{29}Si signal of the T_n groups (Figure 2b″) which shows the maximum at ca. −68 ppm, typical for the formation of T_2 and/or T_3 binding sites [49] that require the hydrolysis of two or three ethoxy groups of the linker. The non-obtained signals of the aliphatic chain of the linker seem to be related to the number of acquired scans which is 16 times lower for the ^{13}C CP MAS DNP SENS spectra compared to the ^{29}Si CP MAS DNP SENS spectrum. Thus, a clear identification of these signals in the presence of signals that are assigned to the polycarbonate foil is not reasonable at the obtained S/N level.

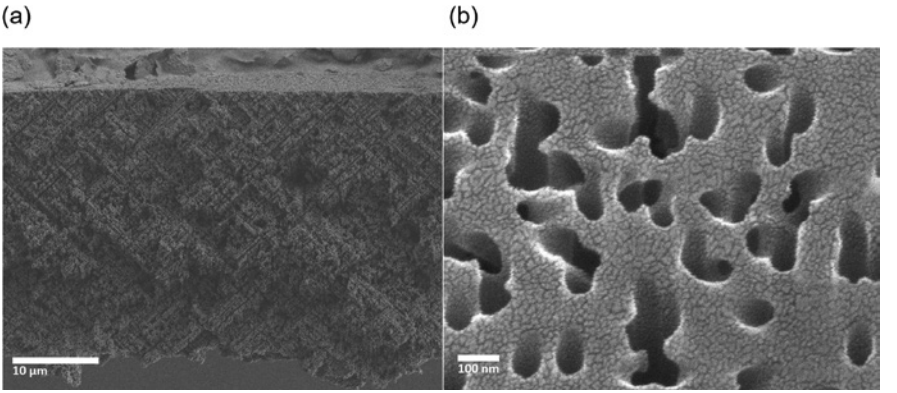

Fig. 4: SEM images of (a) the cross section of a representative polycarbonate etched ion track membrane coated with 20 nm SiO_2 layer revealing the high density of interconnected nanochannels, (b) the top-view of the planar surface of one of the membranes coated with a 5 nm SiO_2 layer subsequently investigated by DNP SENS, and discussed in Figures 2 and 3.

3.4 Surface analysis and scanning electron microscopy (SEM)

Finally, it has been verified that the molecular functionalization of the SiO_2 coated membranes is present along the high aspect ratio nanochannels. Therefore, an estimation of the ratio of the inner-pore surface to the membran planar surface (i.e. excluding the inner-pore surface) was performed (see ESI). This estimation shows that the inner-pore surface is approximately 910 times larger than the membrane surface. Taking into account that the overall specific surface area of the membrane is approximately 25 m^2/g (see ESI) this means that the membrane planar surface is much smaller, namely only 0.027 m^2/g. As such a small surface area is not detectable even with DNP signal enhancement the obtained signals for the functionalization are assumed to stem from groups located on the inner-pore surface.

To underline the surface analysis, SEM images were recorded. Figure 4a displays a SEM cross section of a representative polycarbonate etched ion-track membrane with interconnected channels coated with 20 nm SiO_2 layer by ALD. This image reveals the large inner surface of the channels with respect to the planar surfaces discussed above. An image of the planar surface of the SiO_2 coated membrane used in these experiments is shown in Figure 4b. For the determination of the channels' diameters it has to be taken into account that the channels are tilted by 45° with respect to the surface. It is seen, however, that the observed single channel openings exhibit diameter values that are in good agreement with those

expected from the etching time (~95 nm) minus the thickness of the additional 5 nm SiO_2 layer, i.e. ~85 nm.

3.5 Summary and conclusions

Surface enhanced dynamic nuclear polarization (DNP SENS) has been successfully applied to confirm the surface functionalization of high aspect ratio nanochannels in etched ion-track membranes. The occurrence of T_n groups in the ^{29}Si CP MAS spectra clearly demonstrated the success of the covalent binding of APTES linkers on the surface of SiO_2 coated etched ion-track membranes. By combination of model calculations of pore surfaces, AFM and SEM data it has been verified that the functionalization occurred mostly at the channel surfaces of the SiO_2 coated etched ion-track membranes. The DNP SENS technique provides a novel tool that after suitable adjustment of sample preparation and experimental parameters may be helpful in the future to characterize more complex bioinspired functional etched ion-track membranes.

4 Supporting information

Electronic Supplementary Information (ESI) available: https://doi.org/10.1515/zpch-2017-1032. Additional ^{13}C and ^{29}Si CP MAS spectra, details on approximation of specific surface area of pores, analysis of pore sizes obtained by AFM.

Acknowledgments: This work has been supported by the DFG under contract Bu 911/20-1 (DNP spectrometer) and FOR1583 Grant Nos. Bu 911-18-2, HE 4515/4-2. The authors further thank the project iNAPO by the Hessen State Ministry of Higher Education, Research and the Arts for financial support.

References

1. Z. Ezzeddine, I. Batonneau-Gener, Y. Pouilloux, H. Hamad, Z. Saad, V. Kazpard, Microporous Mesoporous Mater. **212** (2015) 125.
2. Q. Wen, D. Yan, F. Liu, M. Wang, Y. Ling, P. Wang, P. Kluth, D. Schauries, C. Trautmann, P. Apel, W. Guo, G. Xiao, J. Liu, J. Xue, Y. Wang, Adv. Funct. Mater. **26** (2016) 5796.
3. J. Duan, J. Liu, Y. Zhang, C. Trautmann, D. Y. Lei, J. Mater. Chem. C **4** (2016) 3956.
4. I. Schubert, L. Burr, C. Trautmann, M. E. Toimil-Molares, Beilstein J. Nanotechnol. **6** (2015) 1272.

5. G. Pérez-Mitta, C. Trautmann, M. E. Toimil-Molares, O. Azzaroni, Single Ion Track-Etched Nanochannels for Analytical Applications, in "Chemically Modified Nanopores and Nanochannels" (Eds. M. Tagliazucchi, I. Szleifer), William Andrew, Elsevier (2016), P. 61.
6. R. Spohr, Vol. Patent DE 2951376 C2, Germany (1979).
7. A. Mara, Z. Siwy, C. Trautmann, J. Wan, F. Kamme, Nano Lett. **4** (2004) 497.
8. I. Vlassiouk, T. R. Kozel, Z. S. Siwy, J. Am. Chem. Soc. **131** (2009) 8211.
9. K. Healy, B. Schiedt, A. P. Morrison, Nanomedicine **2** (2007) 875.
10. R. L. Fleischer, P. B. Price, R. M. Walker, Nuclear Tracks in Solids: Principles and Applications, University of California Press, Berkeley (1975).
11. A. Spende, N. Sobel, M. Lukas, R. Zierold, J. C. Riedl, L. Gura, I. Schubert, J. M. M. Moreno, K. Nielsch, B. Stuehn, C. Hess, C. Trautmann, M. E. Toimil-Molares, Nanotechnology **26** (2015) 335301.
12. N. Sobel, C. Hess, M. Lukas, A. Spende, B. Stühn, M. E. Toimil-Molares, C. Trautmann, Beilstein J. Nanotechnol. **6** (2015) 472.
13. J. Blümel, Coord. Chem. Rev. **252** (2008) 2410.
14. J. R. Rapp, Y. Huang, M. Natella, Y. Cai, V. S. Y. Lin, M. Pruski, Solid State Nucl. Mag. Res. **35** (2009) 82.
15. J. W. Wiench, Y. S. Avadhut, N. Maity, S. Bhaduri, G. K. Lahiri, M. Pruski, S. Ganapathy, J. Phys. Chem. B **111** (2007) 3877.
16. T. Gutmann, A. Grünberg, N. Rothermel, M. Werner, M. Srour, S. Abdulhussain, S. Tan, Y. Xu, H. Breitzke, G. Buntkowsky, Solid State Nucl. Mag. Res. **55** (2013) 1.
17. M. Geppi, S. Borsacchi, G. Mollica, C. A. Veracini, Appl. Spectrosc. Rev. **44** (2009) 1.
18. H. Koller, M. Weiss, Solid State NMR of Porous Materials Zeolites and Related Materials, in "Solid State NMR", (Ed. J. C. C. Chan), Springer-Verlag, Berlin, Heidelberg, Vol. 306 (2012), P. 189–227.
19. A. Lesage, M. Lelli, D. Gajan, M. A. Caporini, V. Vitzthum, P. Miéville, J. Alauzun, A. Roussey, C. Thieuleux, A. Medhi, G. Bodenhausen, C. Copéret, L. Emsley, J. Am. Chem. Soc. **132** (2010) 15459.
20. R. G. Griffin, Nature **468** (2010) 381.
21. M. Werner, A. Heil, N. Rothermel, H. Breitzke, P. B. Groszewicz, A. S. Thankamony, T. Gutmann, G. Buntkowsky, Solid State Nucl. Magn. Reson. **72** (2015) 73.
22. A. J. Rossini, A. Zagdoun, M. Lelli, A. Lesage, C. Copéret, L. Emsley, Acc. Chem. Res. **46** (2013) 1942.
23. M. Lelli, D. Gajan, A. Lesage, M. A. Caporini, V. Vitzthum, P. Miéville, F. Héroguel, F. Rascón, A. Roussey, C. Thieuleux, M. Boualleg, L. Veyre, G. Bodenhausen, C. Coperet, L. Emsley, J. Am. Chem. Soc. **133** (2011) 2104.
24. W. R. Gruening, A. J. Rossini, A. Zagdoun, D. Gajan, A. Lesage, L. Emsley, C. Coperet, Phys. Chem. Chem. Phys. **15** (2013) 13270.
25. A. Zagdoun, G. Casano, O. Ouari, G. Lapadula, A. J. Rossini, M. Lelli, M. Baffert, D. Gajan, L. Veyre, W. E. Maas, M. Rosay, R. T. Weber, C. Thieuleux, C. Coperet, A. Lesage, P. Tordo, L. Emsley, J. Am. Chem. Soc. **134** (2012) 2284.
26. T. Kobayashi, O. Lafon, A. S. Lilly Thankamony, I. I. Slowing, K. Kandel, D. Carnevale, V. Vitzthum, H. Vezin, J.-P. Amoureux, G. Bodenhausen, M. Pruski, Phys. Chem. Chem. Phys. **15** (**2013**) 5553.
27. E. Pump, J. Viger-Gravel, E. Abou-Hamad, M. K. Samantaray, B. Hamzaoui, A. Gurinov, D. H. Anjum, D. Gajan, A. Lesage, A. Bendjeriou-Sedjerari, L. Emsley, J. M. Basset, Chem. Sci. **8** (2017) 284.

28. M. P. Conley, R. M. Drost, M. Baffert, D. Gajan, C. Elsevier, W. T. Franks, H. Oschkinat, L. Veyre, A. Zagdoun, A. Rossini, M. Lelli, A. Lesage, G. Casano, O. Ouari, P. Tordo, L. Emsley, C. Coperet, C. Thieuleux, Chem. Eur. J. **19** (2013) 12234.
29. T. Gutmann, J. Liu, N. Rothermel, Y. Xu, E. Jaumann, M. Werner, H. Breitzke, S. T. Sigurdsson, G. Buntkowsky, Chem. Eur. J. **21** (2015) 3798.
30. A. Zagdoun, A. J. Rossini, M. P. Conley, W. R. Gruening, M. Schwarzwalder, M. Lelli, W. T. Franks, H. Oschkinat, C. Coperet, L. Emsley, A. Lesage, Angew. Chem. Int. Ed. **52** (2013) 1222.
31. A. R. Mouat, T. Kobayashi, M. Pruski, T. J. Marks, P. C. Stair, J. Phys. Chem. C **121** (2017) 6060.
32. A. J. Rossini, A. Zagdoun, M. Lelli, D. Gajan, F. Rascon, M. Rosay, W. E. Maas, C. Coperet, A. Lesage, L. Emsley, Chem. Sci. **3** (2012) 108.
33. O. Lafon, A. S. L. Thankamony, T. Kobayashi, D. Carnevale, V. Vitzthum, I. I. Slowing, K. Kandel, H. Vezin, J.-P. Amoureux, G. Bodenhausen, M. Pruski, J. Phys. Chem. C **117** (2013) 1375.
34. D. Lee, G. Monin, N. T. Duong, I. Z. Lopez, M. Bardet, V. Mareau, L. Gonon, G. De Paepe, J. Am. Chem. Soc. **136** (2014) 13781.
35. U. Akbey, B. Altin, A. Linden, S. Ozcelik, M. Gradzielski, H. Oschkinat, Phys. Chem. Chem. Phys. **15** (2013) 20706.
36. D. Gajan, M. Schwarzwälder, M. P. Conley, W. R. Gruning, A. J. Rossini, A. Zagdoun, M. Lelli, M. Yulikov, G. Jeschke, C. Sauvee, O. Ouari, P. Tordo, L. Veyre, A. Lesage, C. Thieuleux, L. Emsley, C. Coperet, J. Am. Chem. Soc. **135** (2013) 15459.
37. A. S. L. Thankamony, O. Lafon, X. Y. Lu, F. Aussenac, M. Rosay, J. Trebosc, H. Vezin, J. P. Amoureux, Appl. Magn. Reson. **43** (2013) 237.
38. G. S. Foo, J. J. Lee, C. H. Chen, S. E. Hayes, C. Sievers, C. W. Jones, ChemSusChem **10** (2017) 266.
39. E. Ravera, V. K. Michaelis, T. C. Ong, E. G. Keeler, T. Martelli, M. Fragai, R. G. Griffin, C. Luchinat, Chemphyschem **16** (2015) 2751.
40. T. Kobayashi, D. Singappuli-Arachchige, Z. R. Wang, Slowing, II, M. Pruski, Phys. Chem. Chem. Phys. **19** (2017) 1781.
41. J. Q. Liu, P. B. Groszewicz, Q. B. Wen, A. S. L. Thankamony, B. Zhang, U. Kunz, G. Sauer, Y. P. Xu, T. Gutmann, G. Buntkowsky, J. Phys. Chem. C **121** (2017) 17409.
42. T. Gutmann, B. Kumari, L. Zhao, H. Breitzke, S. Schöttner, C. Rüttiger, M. Gallei, J. Phys. Chem. C **121** (2017) 3896.
43. G. Mollica, D. Le, F. Ziarelli, G. Casano, O. Ouari, T. N. T. Phan, F. Aussenac, P. Thureau, D. Gigmes, P. Tordo, S. Viel, ACS Macro Lett. **3** (2014) 922.
44. P. V. Der Voort, E. F. Vansant, J. Liq. Chromatogr. Relat. Technol. **19** (1996) 2723.
45. A. Spende, PhD Thesis, TU Darmstadt (2016).
46. M. F. P. Wagner, F. Völklein, H. Reith, C. Trautmann, M. E. Toimil-Molares, Phys. Status Solidi B **213** (2016) 610.
47. I. Scholz, P. Hodgkinson, B. H. Meier, M. Ernst, J. Chem. Phys. **130** (2009) 114510.
48. A. E. Bennett, C. M. Rienstra, M. Auger, K. V. Lakshmi, R. G. Griffin, J. Chem. Phys. **103** (1995) 6951.
49. A. Grünberg, X. Yeping, H. Breitzke, G. Buntkowsky, Chem. Eur. J. **16** (2010) 6993.
50. K. Albert, R. Brindle, J. Schmid, B. Buszewski, E. Bayer, Chromatographia **38** (1994) 283.

Supplemental Material: The online version of this article offers supplementary material (https://doi.org/10.1515/zpch-2017-1032).